

*“Perhaps I failed, but I did my best, These masters of mine may
do the rest”*

Nikola Tesla

Declaration

I, *Korobi Konwar*, hereby affirm that this thesis entitled “**Dynamic magnetic responses and quantum phenomena in magnetic ensembles of interacting nanosystems**”, is submitted to School of Sciences, Tezpur University, Tezpur, in partial fulfilment of the requirements for the award of the degree of Doctor of Philosophy in Physics. The thesis is an original record of my own work conducted during Ph.D. term under the supervision of Prof. Pritam Deb. This thesis has never been submitted for any other degree at this or any other University or Institute.

Korobi Konwar

Date: 12-06-2024

Korobi Konwar

Place: Tezpur University

Registration No. TZ201050 of 2019

CERTIFICATE OF THE PRINCIPAL SUPERVISOR



TEZPUR UNIVERSITY

This is to certify that the thesis entitled “**Dynamic magnetic responses and quantum phenomena in magnetic ensembles of interacting nanosystems**”, submitted to the School of Sciences, Tezpur University in partial fulfilment for the award of the degree of Doctor of Philosophy in Physics, is a record of research work carried out by **Ms. Korobi Konwar** under my supervision and guidance. All help received by her from various sources have been duly acknowledged. No part of this thesis has been submitted elsewhere for award of any other degree.

Date: Tezpur University
Place: 12-06-2024



(Principal Supervisor)

Pritam Deb

Professor, Department of Physics
School of Sciences, Tezpur University

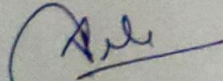
CERTIFICATE OF THE EXTERNAL EXAMINER AND
ODEC



TEZPUR UNIVERSITY

This is to certify that the thesis entitled "Dynamic magnetic responses and quantum phenomena in magnetic ensembles of interacting nanosystems", submitted to the School of Sciences, Tezpur University in partial fulfillment for the award of the degree of Doctor of Philosophy in Physics, is a record of research work carried out by Ms. **Korobi Konwar** under my supervision and guidance.

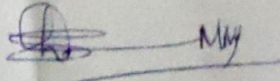
The committee recommends for the award of the degree of Doctor of Philosophy.


Signatures:

Dr. P. Deb
Professor
Dept. of Physics
Tezpur University, Tezpur-784028

Principal Supervisor

Date: 12/06/2024



Prof. M. M. Shaijumon

External Examiner

Date: 12.06.2024

Acknowledgements

First and foremost, I would like to extend my sincere gratitude and appreciation to **Prof. Pritam Deb** for constant guidance, encouragement, valuable research inputs, resources, and has provision of wide range of platforms to represent the research findings at both national and international levels across my doctoral research endeavour. Sir has consistently inspired me to maintain my determination and kept patience while working towards my objectives. Being able to work with him and benefit from his research knowledge while conducting my PhD research is a privilege I greatly appreciate.

I intend to take the opportunity to thank **Dr. Debasis Sen**, Solid State Physics Division, Bhabha Atomic Research Centre (BARC), Mumbai for graciously offering valuable time and expertise during the collaborative work during the visit to BARC. The valuable suggestions during scattering experiments helped me to pursue the work smoothly. I would like to extend my sincere gratitude to **Dr. Som Datta Kaushik**, UGC-DAE-CSR Mumbai Centre, for constant help and support while executing the entire magnetic experiments. Sir has played a major role for executing the thesis objectives. I further acknowledge, **Dr. P. D. Babu**, UGC-DAE-CSR, Mumbai Centre, and **Dr. C. L. Prajapat**, BARC, Mumbai for the help in magnetic experiment. I would like to extend my gratitude to **Dr. Anupam Guleria** and **Dr. Dinesh Kumar**, CBMR, Lucknow, for providing the MRI experimental facilities, and **Prof. Saurabh Lodha**, IIT Bombay, for providing the XPS facilities, **Dr. R. Mukhopadhyay**, MBBT, Tezpur University, for providing cell-viability analysis facility.

I would like to take this opportunity to thank my Doctoral research committee members: **Dr. Rajib Biswas** and **Dr. Ritupan Sarmah** for their invaluable advice, scientific discussions, thorough analysis, and support over the years. Additionally, I would like to thank the Physics Department, Tezpur University for allowing me to pursue my Ph.D. I would like to express my profound gratitude to the entire professors at the Department of Physics, as well as the technical and non-technical personnel, for their assistance and collaboration throughout my Ph.D. I would like to thank **Mr. Narayan Sarma da** for his constant help in the PhD tenure., I would like to thank SAIC, Tezpur University, SAIF NEHU, SAIF CSIR-NEIST, Laboratory of **Prof. D. Mohanta** and **Prof. P. Nath** for providing experimental facilities.

*I would like to acknowledge **UGC-Department of Atomic Energy** for financial support during my PhD in order to perform my PhD smoothly. I also acknowledge **Tezpur University** for providing Institutional Fellowship for financial support for the rest of the PhD tenure. I acknowledge Indian Institute of Technology (IIT) Kharagpur (PARAM SHAKTI) and Centre for Development of Advanced Computing (CDAC), Pune (PARAM SIDDHI) for giving high performing cluster computing (HPCC) facility to execute the high-throughput theoretical simulations.*

*At this moment of accomplishment, I would like to express my heartfelt thanks to **Dr. Koushik Saikia**, for his constant help and guidance during my PhD work, and **Dr. Priyanka Biswas Ba**, BARC, Mumbai for her help during my BARC visit. I would like to acknowledge a few of my teachers from college and masters' days, who has inspired me always: **Dr. Kamal Saharia** Sir, NERIST, **Prof Tado Karlo** Sir, NERIST, and **Deepjaan Gohain** Sir, Lakhimpur Commerce College.*

*I consider myself extremely fortunate to be a member of the Advanced Functional Materials Laboratory (AFML), as I have made many friends and allies there. I would like to thank **Dr. Sushant Kumar Behera** and **Dr. Kashmiri Deka** for any type of scientific conversation, manage lab responsibilities on schedule and with discipline, and have been so encouraging to me during my PhD term that it has really helped me develop personally. I want to specially mention **Mayuri Bora** for always being there as a family and home during my entire PhD tenure and amazed me with her constant encouragement for make the life smooth., and **Dr. Meenakshi Talukdar**, for constant support during these five/six years of my life. Both of them share bundles of sweet memories, scientific/non-scientific discussions, tea discussions, sharing both low and high moments of life and celebrating. Far from home, they made the laboratory feel like home. I would also like to mention my dear junior **Niyorjyoti Sarma**, for always being there through my thick and thin. I would like thank to my dear lab member, **Kashmiri Baruah**, for being such a great personality and friend, and I am always grateful for her support and encouragement at my lows and in celebrating my successes. I would like to thank my dear ex and present lab members: **Monika Sarma**, **Saransha Mohanty**, **Liyenda Gogoi**, **Sayoree Purakayastha**, **Anil K. Singh**, **Deepshekhhar Roy**, **Snehanish**, **Bhagyalakhi Baruah ba**, **Gayatri**, **Saptasindhu**, **Sasanka**, **Oishik**, **Karabi**, **Ritashree**,*

Nayan, Prarthana, Karan, Rozy, Udit, and Bhargav for being such wonderful lab members with their support and encouragement during my challenging phase, also celebrating the achievements.

I am thankful for a few of the great personalities that I have been fortunate enough to meet in my life who constantly uplift me: **Raktim jyoti Sarmah, Mayur Choudhary da, Dr. Amrita Deka ba, Dr. Madhurjya K. Lalung, Rajesh Saikia da, Dr. Duranta Chutia, Bhinnasmita P. Bora, Dhitri Bora, Paramita Deka, Swarnav Buragohain, Ashamoni Neog, Nilav Hazarika, Parishmita Kakoty, Purnima Chakraborty, Nyarik Ete, Imoinu Chanu, Sudhamoyee Kakoty, Rahul Sarma, Suman Paul, Sudip Banik, Naseem Akram, Dr. Hemanga Sarma, Pranjal Bora.** I acknowledge a few seniors and research scholars for their help: **Debabrat da, Swati ba, Saurabh da, Samiran da, Aftab, Stuti, Bhupali, Sunny, Suman, and Deepjyoti.**

A great individual in my life deserves my gratitude, **Rituraj Chakraborty,** for his constant inspiration and support. He continually kept encouraging me to be patient, positive, and determined during my challenging Ph.D. phase. He always glorified my accomplishments. I feel fortunate, blessed, and appreciative to have such upbeat and modest people in my life.

And last not the least, it is my great pleasure to express my deepest admiration and reverence to my beloved parents **Late Probhakor Konwar and Mrs. Bijoya Konwar,** my sister **Dr. Nabanita Konwar,** my brother, **Lakhyajit Konwar,** my brother-in law **Dr. Krishna Dutta,** and my sister-in-law **Bandana Borah** for their unwavering love, support, inspiration, and devotion at my most happy and difficult moments. I cherish them for supporting me and being patient with me while I worked on this thesis for hundreds of hours. Without them it was impossible to achieve the PhD goals.

Date: 12-06-2024

Place: Tezpur University

Korobi Konwar

(Korobi Konwar)

*This Thesis is dedicated to my beloved
parents*

Mrs. Bijoya Konwar

&

Late Probhakar Konwar

List of Tables

Table	Caption	Page no.
Table 2.1	Fitting values achieved via both SAXS and MSANS fitting.	39
Table 3.1	Elementary composition achieved from EDX analysis.	72
Table 4.1	Elementary composition achieved from EDX analysis.	104
Table 5.1	Fitting parameters for primary MNPs from SAXS intensity profile.	133
Table 5.2	Fitting parameters for primary MNPs from SAXS intensity profile.	133
Table 6.1	Fitting of SAXS profile for primary MNPs.	162
Table 6.2	Fitting values from SANS profile for ensembles.	163
Table 7.1	Elementary composition details from EDX analysis.	181
Table 7.2	Fitting values of SAXS intensity profile.	182
Table 7.3	Fitting values of SANS intensity profile.	183
Table 8.1	Elementary composition achieved from EDX analysis.	204
Table 9.1	A comparison of MR-relaxivity efficiency of the developed systems.	221

List of Figures

Figure	Caption	Page no.
Figure 1.1	Schematic of superparamagnetic nanoparticles in absence of any external applied field, in presence of external magnetic field, reversal of superspin in non-interacting superparamagnetic nanoparticles, and an ensemble of interacting superparamagnetic nanosystems.	3
Figure 1.2	Schematic representation of different types of interactions: Dipole-dipole interaction, Exchange interactions: Direct exchange interaction, indirect exchange interaction, RKKY interaction, and super exchange interaction.	5
Figure 1.3	Schematic of frustrated geometry of antiferromagnetic spin, Conventional Spin glass freezing, Cluster Spin glass freezing.	11
Figure 1.4	Schematic on transverse relaxation mechanism and decay period	15
Figure 1.5	(a, b) Longitudinal relaxation enhancement, (c, d) transverse relaxation enhancement.	16
Figure 2.1	Transmission Electron Microscopy (TEM) images of (a, b) Compact Ensemble of Zinc Ferrite (CEZF) and (d, e) Hollow Core Ensemble of Zinc Ferrite (HCEZF), HRTEM images of (c) Compact Ensemble of Zinc Ferrite (CEZF) and (f) Hollow Core Ensemble of Zinc Ferrite (HCEZF). (The nanorods are indicated with yellow arrows in both (c) and (f)). The yellow arrows in Figure (b) indicate the ensemble of CEZF. The yellow arrows in Figure (e) indicate the nanorods assembled on the surface of the ensemble in HCEZF.	36

Figure 2.2	XRD profile of (a) CEZF, (b) HCEZF; SAXS and MSANS intensity profiles of (c) CEZF, (d) HCEZF; MNPs size distribution curve of CEZF (black) and HCEZF (red) in (e) primary MNPs from SAXS, and (f) secondary ensembles achieved from MSANS.	37
Figure 2.3	(a) δM curves of CEZF and HCEZF, (b, c) Irreversible susceptibility curves: (b) CEZF and (c) HCEZF; Zoomed view of field-dependent magnetization: (d) CEZF and (e) HCEZF. Inset (i): Field-dependent magnetization of (d) CEZF and (e) HCEZF. Inset (ii): Law of Approach to Saturation (LAS) fitting of (d) CEZF and (e) HCEZF at 5 K.	40
Figure 2.4	Temperature relying magnetization curve: (a) CEZF and (b) HCEZF. Inset gives Curie-Weiss (CW) model fitting.	43
Figure 2.5	Real component ac susceptibility at $H_{dc} = 0$ kOe and $H_{ac} = 10$ Oe. Inset gives imaginary component ac susceptibility: (a) CEZF, (b) HCEZF. The arrow mark indicates the change in T_{max} and χ_{max} with an increase in frequency.	46
Figure 2.6	(a) Critical slowing down model fitting of CEZF, (b) Critical slowing down model fitting of HCEZF. In inset (i): Arrhenius law of (a) CEZF and (b) HCEZF, and inset (ii): VF model fitting of (a) CEZF and (b) HCEZF. (The error bars in the data represent standard deviation in experimental data).	48
Figure 2.7	(a) Real component ac susceptibility at a field of $H_{dc} = 1$ kOe and $H_{ac} = 10$ Oe; inset gives imaginary component ac susceptibility, (b) Power law; inset gives VF model fitting. (c) Real component ac susceptibility at different fields for HCEZF. The arrow mark in Figure (a) indicates the change in T_{max} and χ_{max} with an increase in frequency and Figure (c) indicates the change in T_{max} with applied DC field. The error bars in the data represent standard deviation in experimental data.	49
Figure 2.8	Field Cooling Magnetic Memory Effects for: (a) of CEZF and (c) HCEZF, (b, d) derivative curve of FC warming plots: (b) CEZF and (d) HCEZF. (e, f) ZFC MME of (e) CEZF and (f) HCEZF. The elliptical shapes indicate the halted temperature region in (a) and (c). The right tick represents the existence of the memory effect. The arrow marks in (e) and (f) indicate the ΔM region.	51

Figure 2.9	(a, b) Ageing relaxation trend with Zero Field Cooling condition for (a) CEZF and (b) HCEZF. (c, d) ageing relaxation trend continuation with stretched exponential model fitting for (c) CEZF and (d) HCEZF.	54
Figure 2.10	A schematic representation of the easy axis in CEZF (left) and HCEZF (right).	56
Figure 3.1	Microstructural study: Core-level X-ray photoelectron spectroscopy (XPS) study (a) Mn 2P, (b) Ni 2P, (c) Fe 2P, (d) O 1s; and (e) XRD pattern of Ensemble of Two-Dimensional flakes (ETD).	69
Figure 3.2	Microstructural study: (a, b) Field Emission Scanning Electron Microscopy (FESEM) images, (c, d) Transmission Electron Microscopy (TEM) images, and (e) Small Angle X-ray Scattering (SAXS) and Small Angle Neutron Scattering (SANS) intensity profile fitting of Ensemble of Two-Dimensional flakes (ETD) (The distribution of Nickel Ferrite nanoparticles is shown in yellow circle in Figure (c)).	71
Figure 3.3	Energy Dispersive X-ray (EDX) microanalysis of Ensemble of Two-Dimensional flakes (ETD): (a) Sum spectrum of all the elements, (b) elementary mapping of Mn, (c) elementary mapping of Ni, (c) elementary mapping of Fe, (d) elementary mapping of O.	73
Figure 3.4	(a) Atomic configuration: the violet, green, golden, and red spheres correspond to manganese (Mn), nickel (Ni), iron (Fe) and oxygen (O), respectively, (b) Electronic band structure, and (c) determination of density of states (DOS) of Ensemble of Two-Dimensional flakes (ETD).	74
Figure 3.5	(a) Spin density distribution with an iso-surface value of 0.0529096 e/Å ³ , (b) Projected density of states (PDOS) individually for iron (Fe), manganese (Mn), nickel (Ni) and oxygen (O), respectively. (c) Electron density distribution with an intensity range of 0 to 1 of Ensemble of Two-Dimensional flakes (ETD).	75
Figure 3.6	DC magnetization of Ensemble of Two-Dimensional flakes (ETD): (a) Field-dependent magnetization study, (b) Zoomed view of hysteresis loop at different temperatures, (c) Law of Approach to Saturation (LAS) fitting at 5 K, 150 K, and 300 K, (d) Random Anisotropy Theory (RAT) fitting at 5 K, 150 K, and 300 K.	76

Figure 3.7	(a) Temperature-dependent magnetization study of Ensemble of Two-Dimensional flakes (ETD) at field 1000 Oe and 100 Oe (The blocking temperature is shown with a downward arrow in both the Zero Field Cooling (ZFC) curve); (b) Curie-Weiss (CW) law fitting and the red fitting line represents the CW law fitting line.	78
Figure 3.8	AC susceptibility (a) in phase, (b) out of phase of Ensemble of Two-Dimensional flakes (ETD). The arrow mark indicates the change in T_{\max} and χ_{\max} with an increase in frequency.	80
Figure 3.9	(a) Arrhenius equation fitting, (b) Vogel-Fulcher (VF) fitting, (c) Critical slowing down model fitting of Ensemble of Two-Dimensional flakes (ETD). The error bars in the data represent standard deviation in experimental data.	83
Figure 3.10	(a) FC magnetic memory effect, (b) Differentiation of FC magnetic memory effect, (c) ZFC magnetic memory effect of Ensemble of Two-Dimensional flakes (ETD).	84
Figure 3.11	(a) Negative T-cycle ZFC ageing, (b) Continuation before and after ageing, (c) Reverse ageing relaxation in ZFC condition and (d) Continuation curve before and after ageing of Ensemble of Two-Dimensional flakes (ETD).	86
Figure 3.12	(a) Reverse T-cycle FC ageing, (b) Continuation before and after ageing, (c) Negative T-cycle in FC condition, and (d) Continuation before and after ageing of Ensemble of Two-Dimensional (2D) flakes (ETD).	87
Figure 3.13	Magnetic relaxation with standard stretched exponent fitting at (a) FC condition, (b) ZFC condition of δ - $\text{MnO}_2@ \text{NiFe}_2\text{O}_4$ (Ensemble of Two-Dimensional (2D) flakes (ETD)).	89
Figure 4.1	Microstructural study: XPS study (a) Mn 2P, (b) Ni 2P, (c) Fe 2P, (d) O 1s; and (e) XRD pattern of α - $\text{MnO}_2@ \text{NiFe}_2\text{O}_4$.	101
Figure 4.2	Micrographs of (a, b) FESEM, (c, d) TEM, (e) SAXS and SANS intensity profile fitting of α - $\text{MnO}_2@ \text{NiFe}_2\text{O}_4$.	102

Figure 4.3	EDX microanalysis of α -MnO ₂ @NiFe ₂ O ₄ : (a) Sum spectrum of the elements, elementary mapping of (b) Mn, (c) Ni, (c) Fe, and (d) O.	103
Figure 4.4	(a) Atomic configuration: the violet, green, golden, and red spheres correspond to Mn, Ni, Fe, and O, respectively, (b) Electronic band structure, and (c) determination of DOS of α -MnO ₂ @NiFe ₂ O ₄ .	105
Figure 4.5	(a) Spin density distribution with an iso-surface value of 0.0529096 e/Å ³ , (b) Projected density of states (PDOS) individually for iron (Fe), manganese (Mn), nickel (Ni) and oxygen (O), respectively. (c) Electron density distribution with an intensity range of 0 to 1 of α -MnO ₂ @NiFe ₂ O ₄ .	106
Figure 4.6	DC magnetization of α -MnO ₂ @NiFe ₂ O ₄ .: (a) Field-dependent magnetization study, (b) Zoomed view of hysteresis loop at different temperatures, (c) Law of LAS fitting at 5 K, 150 K, and 300 K, (d) RAT fitting at 5 K.	107
Figure 4.7	(a) Temperature-dependent magnetization study at field 1000 Oe and 100 Oe (The blocking temperature is shown with a downward arrow in both the Zero Field Cooling (ZFC) curve); (b) Curie-Weiss (CW) law fitting of α -MnO ₂ @NiFe ₂ O ₄ and the red fitting line represents the CW law fitting line.	108
Figure 4.8	AC susceptibility (a) in phase, (b) out of phase of α -MnO ₂ @NiFe ₂ O ₄ . The arrow mark indicates the change in the peak of T _{max} and χ_{max} with an increase in frequency.	111
Figure 4.9	(a) Arrhenius equation fitting, (b) VF fitting, (c) Critical slowing down model fitting of α -MnO ₂ @NiFe ₂ O ₄ . (The error bars in the data represent standard deviation in experimental data).	112
Figure 4.10	(a) Field Cooling (FC) magnetic memory effect at 20 K, 40 K, 60 K, and 80 K, (b) Differentiation of FC magnetic memory effects, (c) Zero Field Cooling (ZFC) magnetic memory effect, ΔM plot, at 40 K (as shown with an arrow) of α -MnO ₂ @NiFe ₂ O ₄ . The elliptical shapes indicate the halted temperature region in Figure (a). The right tick represents the existence of the memory effect.	113

Figure 4.11	(a) Negative T-cycle ZFC ageing, (b) Continuation before and after ageing, (c) Reverse ageing relaxation in ZFC condition, (d) Continuation before and after ageing, (e) Negative FC ageing and (f) Continuation before and after ageing of α -MnO ₂ @NiFe ₂ O ₄ .	115
Figure 5.1	(a) FESEM micrographs of system 1 in scale bar of 100 nm, (b) TEM micrographs of system 1 in scale range of 5 nm, Stable crystal geometry (c) Ni _{0.75} Zn _{0.25} Fe ₂ O ₄ , (d) Ni _{0.75} Zn _{0.25} Fe ₂ O ₄ @CoO, (e) FESEM micrograph of system 2 in scale range of 10 nm, (f) TEM micrograph of system 2 in scale range of 10 nm; stable crystal geometry of (g) Ni _{0.5} Zn _{0.5} Fe ₂ O ₄ , (h) Ni _{0.5} Zn _{0.5} Fe ₂ O ₄ @CoO. For Co, Zn, Ni, Fe, and O, the colour blue, violet, green, golden and red are given.	129
Figure 5.2	(a) XRD plot for (i) system 1, (ii) system 2; (b) SAXS intensity profile fitting for (i) system 1, (ii) system 2; (c) Size distribution plot for system 1, and (d) Size distribution plot for system 2.	130
Figure 5.3	(a) Zeta potential plots for system 1, (b) Zeta potential plots for system 2, pH variation trend with Zeta potential (c) system 1, Ni _{0.75} Zn _{0.25} Fe ₂ O ₄ @CoO, and (d) system 2, Ni _{0.5} Zn _{0.5} Fe ₂ O ₄ @CoO. The error bars in the data is standard deviation in experimental data.	132
Figure 5.4	XPS for Ni _{0.75} Zn _{0.25} Fe ₂ O ₄ @CoO for (a) Co-2P spectrum, (b) Ni-2P spectrum, (c) Zn-2P spectrum, (d) Fe-2P spectrum, and (e) O-1S spectrum; For Ni _{0.5} Zn _{0.5} Fe ₂ O ₄ @CoO for (f) Co-2P spectrum, (g) Ni-2P spectrum, (h) Zn-2P spectrum, (i) Fe-2P spectrum, and (j) O 1S spectrum.	135
Figure 5.5	Electronic band structure as well as DOS calculation for (a, b) Ni _{0.5} Zn _{0.5} Fe ₂ O ₄ , (c, d) Ni _{0.75} Zn _{0.25} Fe ₂ O ₄ . Spin-dependent DOS for: (e) Ni _{0.5} Zn _{0.5} Fe ₂ O ₄ @CoO, (f) Ni _{0.75} Zn _{0.25} Fe ₂ O ₄ @CoO. The given green dashed box is magnified. (g) and (h) depicts the magnified image of core-shell systems.	136
Figure 5.6	Density overlap region indicator (DORI) for (a-c) Ni _{0.5} Zn _{0.5} Fe ₂ O ₄ @CoO: 2D plot and 3D plots at (010) plane, (d-f) Ni _{0.75} Zn _{0.25} Fe ₂ O ₄ @CoO: 2D and 3D plot at (010) plane.	137
Figure 5.7	Field relying magnetization for (a) Ni _{0.75} Zn _{0.25} Fe ₂ O ₄ @CoO, (d) Ni _{0.5} Zn _{0.5} Fe ₂ O ₄ @CoO, Zoomed field relying magnetization for (b) Ni _{0.75} Zn _{0.25} Fe ₂ O ₄ @CoO, (e) Ni _{0.5} Zn _{0.5} Fe ₂ O ₄ @CoO, Asymmetric coercive field for (c)	140

	Ni _{0.75} Zn _{0.25} Fe ₂ O ₄ @CoO, (f) Ni _{0.75} Zn _{0.25} Fe ₂ O ₄ @CoO, LAS fitting for (g) system 1, and (h) for system 2, (i) RAT fit.	
Figure 5.8	Temperature relying magnetization for (a) system 1, (b) system 2; dM/dT plot for (c) system 1, (d) system 2, Curie-Weiss (CW) fitting of (e) system 1, inset gives Griffiths Phase Fitting), (f) system 2 (inset gives Griffiths Phase Fitting). The blocking temperature is denoted in Figure (a, b).	141
Figure 5.9	(a) Real component of ac susceptibility for system 1, (b) Imaginary ac susceptibility of system 2, (c) Real component of ac susceptibility with 1000 Oe dc field for system 1, (d) Imaginary component of ac susceptibility with 1000 Oe field for system 1, (e) Real component ac susceptibility for system 1, (f) Imaginary component ac susceptibility for system 2. The arrow mark indicates the change in the peak of T _{max} and χ _{max} with an increase in frequency. The freezing temperature is denoted in Figure (d).	144
Figure 5.10	MTT assay at HEK cell-line for (a) system 1, and (b) system 2; MTT assay of MCF-7 cell in (c) system 1 and (d) system 2, Inverse longitudinal relaxation plot with metal concentration variation for (e) system 1 and (f) system 2; Inverse longitudinal relaxation time curve with metal concentration variation for (g) system 1 and (h) system 2; Phantom images of longitudinal (i) system 1, (j) system 2; Phantom images at various TE for (k) system 1, and (l) system 2. The error bars in the data present standard deviation in experimental data.	145
Figure 5.11	Schematic for enhancement in transverse relaxivity with variation in exchange field and inhomogeneous anisotropy landscape.	147
Figure 6.1	TEM images of (a, b, c) CEIZF, (d, e, f) CEAIZF (g, h, i) CEZF; (j, k, l) CSEZF, (m, n, o) HCEZF.	160
Figure 6.2	FESEM images of (a) CEIZF, (b) CEAIZF, (c) CEZF, (d) CSEZF, (e) HCEZF.	161
Figure 6.3	SAXS and MSANS fitting (a) CEIZF, (b) CEAIZF, and (c) CSEZF; (d) X-ray Diffraction curves.	162

Figure 6.4	Field relying magnetization: (a) CEIZF, (b) CEAIZF, (c) CSEZF; Zoomed hysteresis pattern view: (d) CEINZF, (e) CEAINZF, (f) CSEZF.	164
Figure 6.5	LAS fitting at temperatures 300 K, 150 K, 30 K, 5 K: (a) CEIZF, (b) CEAIZF, (c) CSEZF.	165
Figure 6.6	Temperature-relying magnetization: (a) CEIZF, (b) CEAIZF, (c) CSEZF ((The blocking temperature is shown with a downward arrow in both the Zero Field Cooling (ZFC) curve); Inset is given for CW-law fitting: (a) CEIZF, (b) CEAIZF, and (c) CSEZF.	166
Figure 6.7	(a) Zeta potential curves in PBS solution, (b) MTT assay for cytotoxicity analysis of HCEZF considering HEK-293.	168
Figure 6.8	(a) r_1 plot at various metal concentrations for CEIZF, CEAIZF, CEZF, CSEZF, HCEZF; (b) r_2 at various metal concentrations for (b) CEIZF, CEAIZF, CEZF, CSEZF, and HCEZF. The error bars in data present standard deviation in experimental data.	168
Figure 6.9	Phantom images for (i) Longitudinal relaxation T_1 : (a) CEIZF, (b) CEAIZF, (c) CEZF, (d) CSEZF, (e) HCEZF; (ii) Transverse relaxation T_2 : (a) CEIZF, (b) CEAIZF, (c) CEZF, (d) CSEZF, and (e) HCEZF.	169
Figure 6.10	A Schematic presentation for varied easy axes in a complex anisotropy landscape and respective faster transverse relaxation trend.	170
Figure 7.1	FESEM micrographs at scale of (a, b, c) 100 nm, (d, e, f, g, h) TEM micrographs, (i) Schematic presentation of complex morphology; the EDX analysis: (j) Sum spectrum for present elements, (k) selected area EDX (30 μ m), (l) for Zinc (Zn), (m) for Iron (Fe), and (n) for Oxygen (O) of γ -Fe ₂ O ₃ @ZnFe ₂ O ₄ . The big hollow ensemble is comprised of elongated shaped nanosystems, which represent the Zinc Ferrite ensemble and the small spherical shapes are used to represent the Iron-Oxide nanoparticles. However, the arrows are marked to illustrate blocked/freeze spins in a certain direction. In Figure (a), the yellow circle is provided to address the Iron Oxide nanoparticles and the red arrow is showing the broken ensemble.	180

Figure 7.2	(a) SAXS and SANS fitting, (b) XRD pattern, (c) Raman plots; XPS study of (d) Zinc 2P, (e) Iron 2P, and (f) Oxygen 1S spectrum of $\gamma\text{-Fe}_2\text{O}_3@\text{ZnFe}_2\text{O}_4$.	184
Figure 7.3	Real component ac susceptibility (a), imaginary component ac susceptibility (b); (c) Arrhenius law fitting, (d) VF law fitting, (e) Critical slowing down fitting of $\gamma\text{-Fe}_2\text{O}_3@\text{ZnFe}_2\text{O}_4$. The arrow mark indicates the change in T_{max} and χ_{max} with an increase in frequency in Figure (a, b). The error bars are for standard deviation representation.	185
Figure 7.4	(a) Zeta potential plot, (b) MTT-assay in HEK-293 cell, (c) MTT-assay in MDA-MB-231 cancer cell; Intensity in signal for both longitudinal relaxation (d), for transverse relaxation (e) at various metal concentrations; (f) $1/T_1$ vs. Metal concentration curve to attain r_1 ; (g) $1/T_2$ vs. Metal concentration to get r_2 of $\gamma\text{-Fe}_2\text{O}_3@\text{ZnFe}_2\text{O}_4$. The error bars are for standard deviation representation.	187
Figure 7.5	Pristine ZnFe_2O_4 : (a) $1/T_1$ vs. Metal concentration curve to attain the longitudinal relaxivity (r_1) and (b) $1/T_2$ vs. Metal concentration to attain the transverse relaxivity (r_2). The error bars in the data represent standard deviation in experimental data.	188
Figure 7.6	(A) Longitudinal relaxivity plot, (B) Transverse relaxivity plot, Phantom images for (i) Longitudinal relaxation with TI, (ii) Transverse relaxation with TE of $\gamma\text{-Fe}_2\text{O}_3@\text{ZnFe}_2\text{O}_4$.	189
Figure 8.1	FESEM images at a resolution (a) $1\ \mu\text{m}$ scale bar, (b) $100\ \text{nm}$ scale bar, (c) $1\ \mu\text{m}$ scale bar, (d) $100\ \text{nm}$ scale bar, and (e) $100\ \text{nm}$ scale bar, and (f) Schematic representation of hybrid ensemble of $\gamma\text{-Fe}_2\text{O}_3@\delta\text{-MnO}_2@\text{NiFe}_2\text{O}_4$. The schematic is depicted wherein three different nanosystems are presented to differentiate among Nickel Ferrite nanoparticles (presented in the core), $\delta\text{-MnO}_2$ nanoflakes, and Iron Oxide nanoparticles over the flakes. Iron Oxide is decorated over the system $\text{MnO}_2@\text{NiFe}_2\text{O}_4$ (which is used in Chapter 3 for magnetic analysis wherein TEM images of $\text{MnO}_2@\text{NiFe}_2\text{O}_4$ are shown). The decoration of Iron Oxide over the ensemble of $\text{MnO}_2@\text{NiFe}_2\text{O}_4$ in yellow circle in Figure (c). The spin arrangement is also shown in the Schematic to illustrate the alignment of the blocked spins.	200

Figure 8.2	(a) SAXS and MSANS intensity profile, (b) XRD curve, and (c) Raman spectrum of $\gamma\text{-Fe}_2\text{O}_3@ \delta\text{-MnO}_2@ \text{NiFe}_2\text{O}_4$.	202
Figure 8.3	XPS analysis for (a) Mn 2P, (b) Ni 2P, (c) Fe 2P, and (d) O 1S spectrum of $\gamma\text{-Fe}_2\text{O}_3@ \delta\text{-MnO}_2@ \text{NiFe}_2\text{O}_4$.	203
Figure 8.4	(a) Sum spectrum of EDX, (b) elementary mapping for O, (c) elementary mapping for Mn, (d) elementary mapping for Fe, and (e) elementary mapping for Ni of $\gamma\text{-Fe}_2\text{O}_3@ \delta\text{-MnO}_2@ \text{NiFe}_2\text{O}_4$.	204
Figure 8.5	(a) In-phase ac susceptibility with different frequencies, (b) out-of-phase ac susceptibility with different frequencies of $\gamma\text{-Fe}_2\text{O}_3@ \delta\text{-MnO}_2@ \text{NiFe}_2\text{O}_4$, (c) depiction of two peaks in out-of-phase component at frequency of 9724 Hz (two different T_{max} are shown in circle). The arrow mark indicates the change in T_{max} and χ_{max} with an increase in frequency in Figure (a, b).	205
Figure 8.6	Temperature maxima fitting with a range of frequency following: (a) Neel-Brown model, (b) VF model, and (c) Critical slowing down model of $\gamma\text{-Fe}_2\text{O}_3@ \delta\text{-MnO}_2@ \text{NiFe}_2\text{O}_4$. The error bars in the data represent standard deviation in experimental data.	206
Figure 8.7	(a) Zeta potential curve, (b) MTT-based cytotoxicity analysis study for HEK-293 cell-line of $\gamma\text{-Fe}_2\text{O}_3@ \delta\text{-MnO}_2@ \text{NiFe}_2\text{O}_4$. The error bars are for standard deviation representation	208
Figure 8.8	MR-relaxation analysis of $\gamma\text{-Fe}_2\text{O}_3@ \delta\text{-MnO}_2@ \text{NiFe}_2\text{O}_4$: (a) Longitudinal relaxivity (r_1) and (b) transverse relaxivity (r_2) plot with various concentrations. The error bars are for standard deviation representation.	208
Figure 8.9	Phantom image of $\gamma\text{-Fe}_2\text{O}_3@ \delta\text{-MnO}_2@ \text{NiFe}_2\text{O}_4$: (i) Longitudinal relaxation at different inversion time (TI) (a-e) and (ii) Transverse relaxation at different echo time (TE) (f-l) with metal concentrations variation.	209
Figure 8.10	Schematic of spin organization in interacting superparamagnetic ensembles having both isotropic and anisotropic MNPs with significant MR-relaxivity of $\gamma\text{-Fe}_2\text{O}_3@ \delta\text{-MnO}_2@ \text{NiFe}_2\text{O}_4$.	210

List of Symbols

Parameters	Meanings
\AA	Angstrom, atomic scale unit
nm	Nanometer
M_s	Saturation magnetization
k_B	Boltzmann constant
M_r	Remanence
q	Scattering vector
T_B	Blocking Temperature
emu	electromagnetic units
σ	Polydispersity index
K	Magnetic anisotropy constant
$n(r)$	Density of states
T_B	Blocking temperature
T_f	Freezing temperature
T_g	Glass transition temperature
E_F	Fermi energy
Ry	Rydberg constant
τ	Spin flipping time
T_1	Longitudinal relaxation time
T_2	Transverse relaxation time
r_1	Longitudinal relaxivity
r_2	Transverse relaxivity
T_C	Curie Temperature
γ_0	Proton gyromagnetic ratio
$\Delta\omega$	Larmor frequency
τ_{diff}	Diffusive time

Abbreviations Names

MNPs	Magnetic Nanoparticles
2D	Two-dimension
SAXS	Small Angle X-ray Scattering
SANS	Small Angle Neutron Scattering
DBF Model	Dormann-Bessais-Fiorani Model
MT Model	Mørup-Tronc Model
FC	Field Cooling
ZFC	Zero Field Cooling
DFT	Density Functional Theory
DLS	Dynamic Light Scattering
HRTEM	High Resolution Transmission Electron Microscopy
DOS	Density of states
VF	Vogel-Fulcher
MRI	Magnetic Resonance Imaging
PPMS	Physical Property Measurement System
TI	Inversion Time
TE	Echo Time
TD-NMR	Time Domain Nuclear Magnetic Resonance
mM	Milimole
DCD	Direct current demagnetization
LDA	Local Density Approximation
RF	Radio frequency
QE	Quantum Espresso
PP	Pseudopotential
RKKY	Ruderman-Kittel-Kasuya-Yosida
SSG	Super spin glass
SPM	Superparamagnetism
NaOH	Sodium Hydroxide
DMSO	Dimethylsulfoxide
FESEM	Field Emission Scanning Electron Microscopy
PVP	Polyvinylpyrrolidone
DM	Dzyaloshinskii-Moriya
XRD	X-ray Diffraction
SDR	Static Dephasing Regime
MAR	Motional Averaging Regime
SBM	Soloman-Bloembergen-Morgan
MME	Magnetic Memory Effect
PDOS	Partial density of states
AFM	Antiferromagnetic
FM	Ferromagnetic
BZ	Brillouin Zones

PW	Perdew and Wang
LDA	Local Density Approximation
RRKJ	Rappe-Rabe-Kaxiras-Joannopoulos
USPP	Ultrasoft Pseudopotentials
KS	Kohn-Sham
BFGS	Broyden-Fletcher-Goldfarb-Shanno
DMEM	Dulbecco's Modified Eagle Medium
HEK-293	Human Embryonic Kidney cell lines
MCF-7	Michigan Cancer Foundation cell lines
MTT	3-(4,5-Dimethylthiazol-2-yl)-2,5-Diphenyltetrazolium Bromide
JCPDS	Joint Committee on Powder Diffraction Standards